Experimental and Model Studies of Oscillations, Photoinduced Transitions, and Steady States in the $Ru(bpy)_3^{2+}$-Catalyzed Belousov−Zhabotinsky Reaction under Different Solute Compositions

Takashi Amemiya,*,† Tetsuya Yamamoto,‡ Takao Ohmori,§ and Tomohiko Yamaguchi*,†

Nanotechnology Research Institute, National Institute of Advanced Industrial Science and Technology (AIST), Tsukuba Central 5, 1-1-1 Higashi, Tsukuba, Ibaraki 305-8565, Japan, and Research Institute for Green Technology, National Institute of Advanced Industrial Science and Technology (AIST), Tsukuba Central 5, 1-1-1 Higashi, Tsukuba, Ibaraki 305-8565, Japan

Received: July 16, 2001; In Final Form: October 26, 2001

Experiments of the $Ru(bpy)_3^{2+}$-catalyzed Belousov−Zhabotinsky (BZ) reaction exhibited several types of oscillations, photoinduced transitions, and steady states in a continuous-flow stirred tank reactor (CSTR) system under a wide range of oxidative and reductive solute conditions. An improved Oregonator-class model of the photosensitive BZ reaction has reproduced the experimental behavior quantitatively as well as other photoinduced behavior reported so far.

I. Introduction

Studies of the $Ru(bpy)_3^{2+}$-catalyzed Belousov−Zhabotinsky (BZ) reaction[1−3] have shown a variety of photoinduced behavior including photoinhibition[4−8] (transitions from oscillations to steady sates), photoinduction[6,9] (transitions from steady states to oscillations), and irregular oscillations[7] under constant irradiation of light. Pulsed-light irradiation has exhibited quenching of oscillations,[10] phase-shifts in oscillations,[11−13] and induction of excitability.[14] All the photoinduced behavior is known to depend largely on the solute compositions.[9,15] Kinetic studies of the photosensitive BZ system[8,9,14,16] and of the $Ru(bpy)_3^{2+}$-catalyzed minimal bromate system[17−19] have proven that light works either as inhibitory or as accelerative depending on the solute compositions; the photoexcited catalyst $*Ru(bpy)_3^{2+}$ has been confirmed to produce both Br^- (an inhibitor) from the reduction of bromomalonic acid ($CHBr(COOH)_2$, abbreviated to BrMA), and $BrO_2^\bullet$ (an accelerator) form the reduction of bromate (BrO_3^-) via two separate photochemical reaction steps.[8]

Model studies of the $Ru(bpy)_3^{2+}$-catalyzed BZ reaction have been carried out in terms of both the detailed chemical reaction mechanisms[20−22] and the simplified scheme of the reaction, i.e., the Oregonator model.[23] Gao and Försterling[24] proposed a detailed model to simulate the oscillatory behavior for the $Ru(bpy)_3^{2+}$/BrMA/BrO_3^-/H_2SO_4 system. Zeyer and Schneider[25] have subsequently extended the above model to that composed of 19 reaction steps and 16 variables and have succeeded in reproducing almost all of the oscillatory behavior in the $Ru(bpy)_3^{2+}$-catalyzed BZ reaction under dark and flow conditions. The Oregonator model has also been used to simulate behavior of several types of fluorescence oscillations,[26] and phase shifts in oscillations induced by light pulse.[13] To account for the effects of light on the $Ru(bpy)_3^{2+}$-catalyzed BZ reaction, Kádár et al.[8] have modified the Oregonator model based on the two photochemical reaction steps mentioned above. The modified three-variable ($X = [HBrO_2]$, $Y = [Br^-]$, $Z = [Ru(bpy)_3^{3+}]$) Oregonator model, in which the concentration of [BrMA] was considered to be constant, has reproduced the photoinhibition in a batch system,[8] and further, the model with flow terms has also exhibited photoinduction under conditions of high flow rates and high values of the ratio of $[BrO_3^-]$/[BrMA].[27,28] Recently, this three-variable model has been extended to a four-variable ($X = [HBrO_2]$, $Y = [Br^-]$, $Z = [Ru(bpy)_3^{3+}]$, and $V = [BrMA]$) model[29] in order to cover a condition where BrMA does not exist initially, instead is accumulated in the course of the BZ reaction. This Oregonator-class model[29] has been found to exhibit much variety of the photoinduced behavior in agreement with the experiments. However, the following three points were still unrealistic: (i) the system may exhibit oscillations with the values of Z exceeding the total concentration of the catalyst under high concentrations of BrO_3^- and H^+, (ii) the values of V may also exceed the initial concentration of malonic acid ($CH_2(COOH)_2$, abbreviated to MA) from which BrMA is formed, and (iii) the model system can absorb light infinitely independent of the concentration of the light absorbing species $Ru(bpy)_3^{2+}$.

The present study has two aims; one is to examine experimentally the dependence of the system behavior in the $Ru(bpy)_3^{2+}$-catalyzed BZ reaction, i.e., oscillations, photoinduced transitions, and steady states, on the solute compositions, and the other is to improve the previous Oregonator-class model[29] so as to reproduce the present experimental results as well as the already reported behavior under the realistic constraints. The solute compositions have been varied over a wide range of oxidative and reductive conditions; the ratio of $[BrO_3^-]$ to that of [MA] has been changed over 3 orders of magnitude.

II. Experimental Section

Commercially available analytical grade reagents (H_2SO_4, $NaBrO_3$, NaBr, $CH_2(COOH)_2$, and $(NH_4)_2Ce(NO_3)_6$) were used without further purification. The $Ru(bpy)_3Cl_2(6H_2O)$ was converted into $Ru(bpy)_3SO_4(H_2O)$ according to the literature.[24,25]

* To whom correspondence should be addressed. E-mail: t-amemiya@aist.go.jp, tomo.yamaguchi@aist.go.jp. Fax: +81−298−61−4652.

† Nanotechnology Research Institute, National Institute of Advanced Industrial Science and Technology (AIST).

‡ Permanent address: Department of Electrical Engineering, Tokyo Metropolitan College of Technology, Shinagawa, Tokyo 140-011, Japan.

§ Research Institute for Green Technology, National Institute of Advanced Industrial Science and Technology (AIST).

10.1021/jp012717u CCC: $22.00
Published on Web 01/05/2002

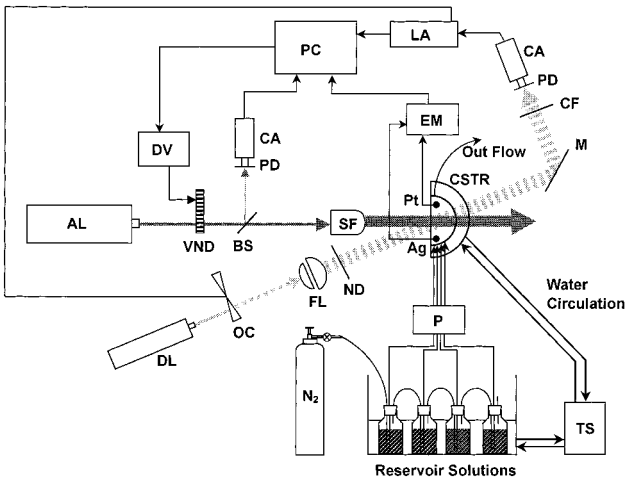

Figure 1. Schematic drawing of the experimental setup: AL, argon ion laser; VND, variable neutral-density filter; DV, driver; BS, beam sampler; SF, spatial filter assembly; DL, diode laser; OC, optical chopper; FL, focusing lenses; ND, neutral-density filter; M, mirror; CF, color filter; PD, photodiode; CA, current amplifier; LA, lock-in amplifier; PC, personal computer; Ag, Ag-electrode; Pt, Pt-electrode; EM, electrometer; N_2, nitrogen gas cylinder; P, peristaltic pump; TS, thermostat.

Highly purified water (Elga, UHQ-PS) was used to prepare the following stock solutions: 6 M H_2SO_4, 1.5 M $NaBrO_3$, 0.1 M NaBr, 3 M $CH_2(COOH)_2$, 30 mM $(NH_4)_2Ce(NO_3)_6$, and 36 mM Ru(bpy)$_3$SO$_4$. The concentration of stock solution of Ru(bpy)$_3$SO$_4$ was determined spectrophotometrically ($\epsilon_{460\ nm}$ = 11350 M^{-1} cm^{-1}).[25] The solution of $(NH_4)_2Ce(NO_3)_6$ was used to oxidize Ru(bpy)$_3^{2+}$ to Ru(bpy)$_3^{3+}$.

The experimental setup is shown in Figure 1. The experiment was carried out in a continuous-flow stirred tank reactor (CSTR) system. A semicylindrical glass reactor of 9 mL in volume and 4.5 cm in height was surrounded by water jacket except for one side of the reactor that was a flat optical window for light irradiation. Four solutions in reactant reservoirs, $NaBrO_3$ in H_2O, NaBr in H_2SO_4, $CH_2(COOH)_2$ in H_2SO_4, and Ru(bpy)$_3$SO$_4$ in H_2O, were prepared from the stock solutions by diluting with the purified water. The solutions were introduced into the reactor from the bottom through Tygon tubes by a peristaltic pump (Ismatec, IPC-4) at a flow rate of 1.38×10^{-3} s^{-1} (residence time of 12 min). The reaction mixture was vigorously stirred by a Teflon-coated magnetic stirrer bar, and flowed out from the top of the reactor through a Tygon tube. The concentrations of the in-flow were changed over a wide range of oxidative and reductive conditions by varying the concentrations of $NaBrO_3$ and $CH_2(COOH)_2$, whereas the other concentrations remained constant as listed in Table 1. The solutions in the reservoirs were bubbled by nitrogen gas for 15 min prior to use, and maintained under a very slow bubbling of nitrogen gas during the experiment. The temperature of both the reservoir solutions and the reactor was maintained at 25.0 ± 0.1 °C by using a thermostat (Yamato-Komatsu, Coolnics CTR42AS).

The optical system was set up with reference to that reported by Okazaki et al.[30] The light source was a 500 mW tunable argon ion laser (Omnichrome, 543−500MA) that emits light wavelengths of mainly 488 and 514.5 nm. The laser power was set to a constant value of 350 mW maintained by an internal optical feed back circuit in the laser system. The incident light intensity was controlled by a continuously variable neutral-density (VND) filter (Sigma Koki, Σ-78A-100PM) equipped with a driver (Sigma Koki, CSG-501) controlled by a personal computer with an attached board (Hachinohe Firmware System,

TABLE 1: Solute Concentrations of the In−Flow (Reservoir Concentrations Divided by Four) in the CSTR System[a]

run	[BrO_3^-] (M)	[$CH_2(COOH)_2$] (M)	[BrO_3^-]/[$CH_2(COOH)_2$] (−)
a	0.13	0.002	65
b	0.13	0.009	14.4
c	0.08	0.08	1
d	0.08	0.6	0.13
e	0.065	1	0.065

[a] Concentrations of the other chemicals were constant: [H_2SO_4] = 0.6 M, [Ru(bpy)$_3^{2+}$] = 0.1 mM, and [Br^-] = 0.05 mM. The flow rate was 1.38×10^{-3} s^{-1}.

GPIB-DLII and 12A/D-DL). The laser beam of 0.66 mm in diameter first passed through the VND filter, and was expanded through a spatial filter assembly (Melles Griot, 07SFM001) equipped with a set of focusing lenses. The expanded beam of 11 mm in diameter irradiated the reaction mixture normal to the optical window. The light intensity at the window was calibrated with a laser power meter (Neo Ark, PM-311).

Small amount (4∼6%) of the incident beam was taken with a beam sampler (Sigma Koki, BS4−30C05−10W-550) just behind the VND filter and was continuously monitored with a photodiode (Hamamatsu, S2281−01) equipped with a current input preamplifier (NF Electronic Instruments, LI-76). The incident light intensity was calibrated to the sampled light intensity prior to each experiment. This optical system allowed us to scan the light intensity with a desired time profile. The sampled light intensity was recorded on the computer during the experiments.

The reaction mixture was monitored both with an electrode system composed of Pt-working and Ag-quasi-reference electrodes for the redox potential and with light of 635 nm from a 5mW diode laser (Point Source, iFLEX-1000) for the absorption due to Ru(bpy)$_3^{3+}$. The two electrodes were immersed into the solution vertically from the top, and were located so as not to interfere with the optical paths for the two laser beams. The redox potentials were detected with an electrometer (Hokuto Denko, HE−104), and the output signals were recorded on the computer. The monitoring laser beam of 635 nm was modulated with an optical chopper (Scitec Instruments) at 170 Hz to employ a lock-in technique. The diameter of the beam was expanded from 0.65 mm to 10 mm through a set of two focusing lenses. The expanded beam passed through another neutral-density (ND) filter, and reached the window of the reactor with an incident angle of about 30°. The intensity of the beam transmitted through the reactor was monitored with a photodiode (Hamamatsu, S2281−01) equipped with a color filter (Sigma Koki, SCF-50S-58O) that cut off the scattered light from the argon ion laser. Photocurrent signals from the photodiode were amplified with a current input preamplifier (NF Electronic Instruments, LI-76), and the output signals from the preamplifier were further amplified with a two-phase lock-in amplifier (NF Electronic Instruments, 5610B) with a time constant of 100 ms that was much shorter than the time scale of the BZ oscillations. The output signals from the lock-in amplifier were recorded on the computer.

The concentrations of Ru(bpy)$_3^{3+}$ (C) in the reactor were calculated from the intensity (D) of the monitoring beam transmitted through the reactor by using the Beer−Lambert law

$$C = C_{ox}\frac{\log (D_0/D)}{\log (D_0/D_{ox})} \qquad (1)$$

where C_{ox} is a known concentration (0.1 mM) of Ru(bpy)$_3^{3+}$

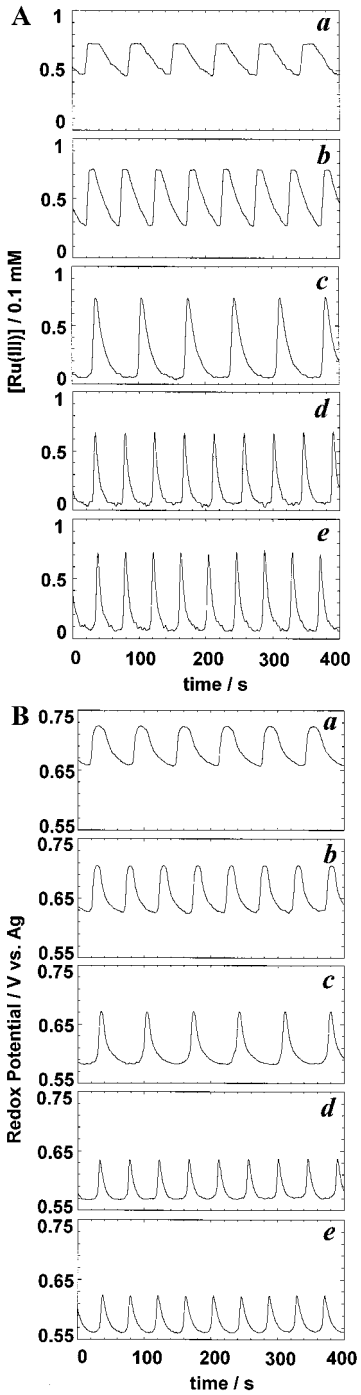

Figure 2. Experimental results of oscillatory behavior in concentrations of $Ru(bpy)_3^{3+}$ (abbreviated as Ru(III) in the figure) (A), and redox potentials (B) under dark conditions. Charts a, b, c, d, and e correspond to the experimental runs listed in Table 1.

that was oxidized by 1 mM of $(NH_4)_2Ce(NO_3)_6$ in 0.3 M H_2SO_4 solution; D_{ox} and D_0 are the intensities of the beam transmitted through the oxidized solution and pure water, respectively.

III. Experimental Results

Oscillations under Dark Conditions. Reactions carried out under different solute compositions exhibited oscillations that depended on the solute compositions as shown in Figure 2. The data shown in Figure 2 were stationary oscillations recorded at 30 min after running the inflow of the reservoir solutions. Under a highly oxidative condition (chart a), the oscillations exhibited a plateau in an oxidized state. This plateau was observed more clearly in the optical transmittance, i.e., the concentrations of $Ru(bpy)_3^{3+}$ (Figure 2A), than in the redox potentials (Figure 2B). A Similar plateau has been observed in the ferroin-catalyzed BZ system[31,32] and in the $Ru(bpy)_3^{2+}$-catalyzed BZ system in gel[33] with optical measurements. As the solute compositions were changed from oxidative to reductive conditions, the plateau became narrow (chart b), and the oscillations exhibited sharp waveforms (charts c, d, e).

Oscillations and Steady-State Behavior under Irradiated Conditions. The oscillations under laser irradiation were shown in Figure 3. The irradiation was started after recording the oscillations under dark conditions, i.e., at 60 min after running the inflow of the solutions, and the laser intensity at the optical window of the reactor was changed linearly from 0 to 80 mW/cm^2 over a period of 60 min. The increase in the beam intensity induced a variety of transitions from oscillatory to steady state behavior that depended on the solute compositions. Under a highly oxidative condition (chart a), the amplitude of oscillations gradually became smaller, and the system exhibited steady-state behavior in an oxidized state (not shown). Here, the oxidized steady state was defined as $[Ru(bpy)_3^{3+}] \geq C_0/2$, where C_0 (= 0.1 mM) is the total concentration of the catalyst. Abrupt transitions from oscillatory to steady state behavior were shown under different solute compositions (charts b and c). These systems remained in an oxidized steady state (chart b) and in a reduced steady state (chart c), respectively. A more reductive solute composition exhibited a different type of transitions from oscillatory to steady state behavior (chart d); several oscillations with small amplitudes were demonstrated just before the transitions. This system remained in a reduced steady state after the oscillations were stopped. Under a highly reductive solute composition (chart e), the transition from oscillatory to steady state behavior was smooth; the amplitudes of oscillations gradually became small, and the system eventually showed no oscillations and remained in a reduced steady state.

IV. Model

To simulate the experimental results quantitatively, we have improved an Oregonator-class model proposed previously.[29] The chemical reaction steps in the present model are listed in Table 2. We have made three improvements on the previous model: (i) the third step (O3) of the Oregonator model[23] is replaced by two steps (O3a and O3b) that introduce the additional species W (= $[BrO_2^{\bullet}]$) and the reduced form of the catalyst G (= $[Ru(bpy)_3^{2+}]$) as proposed by several authors.[34−36] The reaction of G with W provides a stoichiometric constraint, $C_0 - Z$, so that Z (= $[Ru(bpy)_3^{3+}]$) cannot become larger than the total concentration (C_0) of the catalyst. The introduction of W also improves the photochemical reaction step; the photoinduction reaction L2′ as listed in Table 2 was replaced by the sum of the steps O3a and L2′ in the previous paper.[8,27−29] (ii) the production of V (= [BrMA]) is represented by step O6 in which BrMA is generated from P (= [HOBr]) with a stoichiometric factor g (= $1 - V/B_0$), where B_0 is the initial or in-flow concentrations of MA. This stoichiometric factor denotes the normalized concentration of MA, and is introduced to represent the depletion of MA that reacts with HOBr to produce BrMA.[37] This factor also satisfies the experimental constraint on V ($V \leq B_0$). In addition, we introduce quasi-steady-state approximation for P (see Table 2 and VI Discussion section). (iii) the concentration of the light absorbing species $Ru(bpy)_3^{2+}$ is taken into account in the primary photochemical reaction step L0 according to Hanazaki.[38] The photoexcitation rate is given by

$$\left(\frac{dE}{dt}\right)_{ext} = \frac{\sigma_0}{h\nu} GI \tag{2}$$

where E is the concentration of *Ru(bpy)$_3^{2+}$, σ_0 (cm^2) is the collision cross section of a photon with a molecule Ru(bpy)$_3^{2+}$, $h\nu$ (J s) is photon energy, and I (W cm^{-2}) is light intensity.[38] The values of these physical quantities (σ_0, $h\nu$, and I) depend on wavelengths of light in the experiments, i.e., 488 and 514.5 nm, however, in the present model, the product $(\sigma_0/h\nu)I \equiv \Psi$ (s^{-1}) is treated as one control parameter that is assumed to be proportional to the light intensity.

The overall photochemical reaction in the present model consists of steps L0, L1, and L2′. Steady-state approximation for E can eliminate E from the reaction rates for steps L1 and L2′ as given in Table 2, which is described in the previous paper in detail.[29] It is noted that the photoexcitation rate of Ru(bpy)$_3^{2+}$ in the primary photochemical reaction step L0 was equal to light flux Φ (M s^{-1}) in the previous paper, however, is replaced by $(\sigma_0/h\nu)GI \equiv G\Psi \approx (C_0 - Z)\Psi$ (M s^{-1}) that is a function of light intensity and the concentration of the reduced or oxidized form of the catalyst.

The present model gives the differential equations as shown in Table 3, which are briefly expressed by

$$\frac{d\boldsymbol{X}}{dt} = \boldsymbol{A} + \boldsymbol{F}\, k_f + \boldsymbol{P}\Psi \tag{3}$$

where d$\boldsymbol{X}$/dt is the production rate of X, Y, Z, W, and V; $\boldsymbol{A}$ is the kinetic term of the present model, $\boldsymbol{F}k_f$ is a flow term with a flow rate of k_f, and $\boldsymbol{P}\Psi$ is the photochemical term with apparent light intensity Ψ. The photochemical terms $p_1(V,Z)$ and $p_2(V,Z)$ are a function of V and Z as shown in Table 3. Note that the variable V involves in the dynamics only under irradiated conditions, thus the present five-variable model can be reduced to the four-variable (X, Y, Z, and W) version of the original Oregonator model under dark conditions. The rate equations of the present model were numerically integrated to simulate the experimental results by using the values of the rate constants[36] and of parameters as listed in Table 4.[39] In the simulations, the solute concentrations and the flow rate were the same as those in the experiments. Adjustable parameters were the rate constant k_{O5} and the stoichiometric factor h, and these values were optimized in each run as listed in Table 4.

V. Numerical Results

Oscillations under Dark Conditions. The simulated behavior under dark conditions is shown in Figure 4. To simulate the behavior in the redox potential, the function of $f(Z) = (RT/F)\ln(Z/(C_0 - Z))$ was used; where R is the gas constant, F is the Faraday constant, and T is the absolute temperature. The numerical results obtained from the present model agreed with the experimentally observed behavior; oscillations with a plateau in an oxidized state under the highly oxidative solute composition (chart a), change in the waveforms from oxidative to reductive solute compositions (charts b−e), and the concentration range in oscillations.

Oscillations and Steady-State Behavior under Irradiated Conditions. Simulations under the irradiated conditions also exhibited good agreement with the experimental results as shown in Figure 5. The characteristic transitions from oscillatory to steady-state behavior, i.e., the abrupt and smooth transitions, were reproduced well. The dependence of the critical light intensities, for which the oscillations did not occur, on the solute compositions was also simulated well; the critical light intensity was higher for the more oxidative solute compositions.

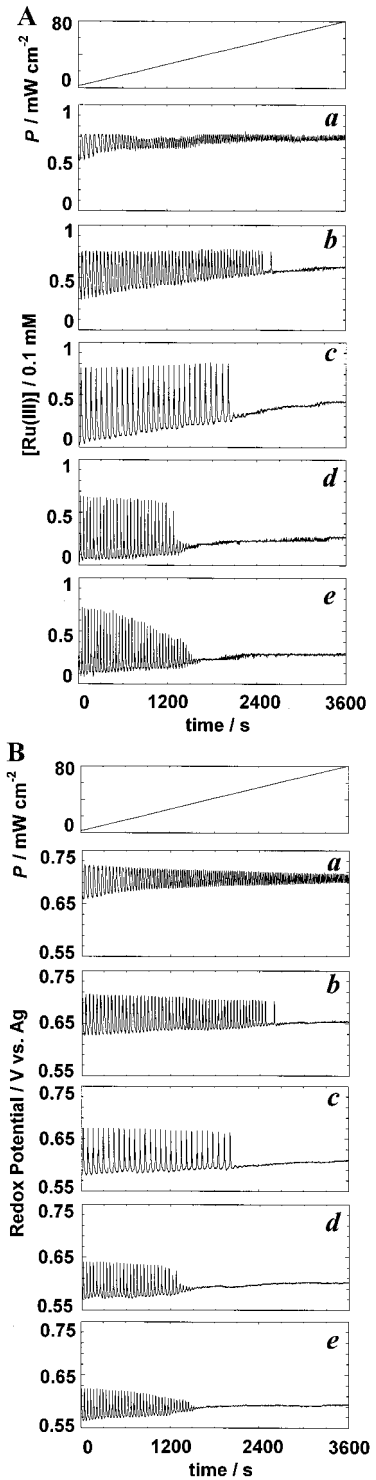

Figure 3. Experimental results of transitions from oscillatory to steady-state behavior in concentrations of Ru(bpy)$_3^{3+}$ (abbreviated as Ru(III) in the figure) (A), and in redox potentials (B) under laser irradiation. The laser power at the optical window of the reactor was changed linearly as shown in the top chart in this figure. Charts a, b, c, d, and e correspond to the experimental runs listed in Table 1.

State Diagram Spanned by Light Intensity and Flow Rate. A state diagram spanned by light intensity and flow rate under the condition b in Table 1 is shown in Figure 6. The state diagram was constructed from the behavior of Z, and was found to be divided into three regions: oscillatory states, oxidized steady states, and reduced steady states. Under low flow rate

TABLE 2: Chemical Reaction Steps and Reaction Rates of a Five-Variable Oregonator-Class Model for the Photosensitive BZ Reaction

	chemical reaction steps	reaction rates: forward	reaction rates: reverse	note
(O1)	$A + Y \rightarrow X + P$	$r_{O1} = k_{O1} A Y$		
(O2)	$X + Y \rightarrow 2\,P$	$r_{O2} = k_{O2} X Y$		
(O3a)	$A + X \leftrightarrow 2W$	$r_{O3a} = k_{O3a} A X$	$r_{-O3a} = k_{-O3a} W^2$	
(O3b)	$G + W \rightarrow X + Z$	$r_{O3b} = k_{O3b} (C_0 - Z) W$		
(O4)	$2\,X \rightarrow P + A$	$r_{O4} = k_{O4} X^2$		
(O5)	$Z \rightarrow h\,Y$	$r_{O5} = k_{O5} Z$		
(O6)	$P \rightarrow g\,V$	$r_{O6} = k_{O6} P$		*a*, *b*
(O7)	$V \rightarrow$ products	$r_{O7} = k_{O7} V$		
(L0)	$G \leftrightarrow E$	$r_{L0} = (C_0 - Z)\,\Psi$	$r_{-L0} = k_{-L0} E$	*c*
(L1)	$E + V + H \rightarrow Y + Z$	$r_{L1} = k_{L1} E V H$		*c*
(L2′)	$E + A + 2\,H \rightarrow W + Z$	$r_{L2'} = k_{L2'} E A H^2$		*c*, *d*

Variables: $X = [HBrO_2]$, $Y = [Br^-]$, $Z = [Ru(bpy)_3^{3+}]$, $W = [BrO_2^\bullet]$, $V = [CHBr(COOH)_2]$. Constants: $A = [BrO_3^-]$, $H = [H^+]$, $C_0 = [Ru(bpy)_3^{3+}] + [Ru(bpy)_3^{2+}] + [*Ru(bpy)_2^{2+}] \approx [Ru(bpy)_3^{3+}] + [Ru(bpy)_3^{2+}] = Z + G$. [a] A stoichiometric factor g ($= 1 - V/B_0$), which represents the normalized concentration of malonic acid B ($= [CH_2(COOH)_2]$), is introduced to meet the experimental constraint on $V \le B_0$ where B_0 is the initial or in-flow concentration of B (see text, IV Model and VI Discussion sections). [b] Quasi-steady-state approximation for P ($= [HOBr]$) gives the rate in step O6 as $k_{O6}\,P \approx k_{O1}\,A\,Y + 2\,k_{O2}\,X\,Y + k_{O4}\,X^2$ (see text, VI Discussion section). [c] Steady-state approximation for the photoexcited catalyst $E = [*Ru(bpy)_2^{2+}]$ can eliminate E from these rates: $dE/dt = (C_0 - Z)\,\Psi - k_{-L0}\,E - k_{L1}\,E\,V\,H - k_{L2'}\,E\,A\,H^2 \approx 0$. Ψ: apparent light intensity (s^{-1}) (see text, IV Model and VI Discussion sections). [d] The rate constant $k_{L2'}$ is the same as k_{L2} in the previous paper, because step L2′ was assumed to be rate determining in step L2 in the previous paper.[29]

TABLE 3: Differential Equations for the Five-Variable Oregonator-Class Model for the Photosensitive BZ Reaction

$$\begin{Bmatrix} dX/dt \\ dY/dt \\ dZ/dt \\ dW/dt \\ dV/dt \end{Bmatrix} = \begin{Bmatrix} k_{O1}AY - k_{O2}XY - k_{O3a}AX + k_{-O3a}W^2 + k_{O3b}(C_0 - Z)W - 2k_{O4}X^2 \\ -k_{O1}AY - k_{O2}XY + hk_{O5}Z \\ k_{O3b}(C_0 - Z)W - k_{O5}Z \\ 2k_{O3a}AX - 2k_{-O3a}W^2 - k_{O3b}(C_0 - Z)W \\ (1 - V/B_0)(k_{O1}AY + 2k_{O2}XY + k_{O4}X^2) - k_{O6}V \end{Bmatrix} + \begin{Bmatrix} -X \\ -(Y - Y_{in}) \\ -Z \\ -W \\ -(V - V_{in}) \end{Bmatrix} k_f + \begin{Bmatrix} 0 \\ p_1(V,Z) \\ p_1(V,Z) + p_2(V,Z) \\ p_2(V,Z) \\ -p_1(V,Z) \end{Bmatrix} \Psi$$

Flow terms:
Y_{in}: in-flow concentration of Y
V_{in}; in-flow concentration of V (zero in the present study)
Photochemical terms: calculated from the reaction rates in Table 2 by using the steady-state approximation for E.

$$p_1(V,Z) = \frac{HV(C_0 - Z)}{\frac{k_{-L0}}{k_{L1}} + HV + \frac{k_{L2'}}{k_{L1}}H^2A}, \qquad p_2(V,Z) = \frac{\frac{k_{L2'}}{k_{L1}}H^2A(C_0 - Z)}{\frac{k_{-L0}}{k_{L1}} + HV + \frac{k_{L2'}}{k_{L1}}H^2A}$$

conditions, increase in the light intensity induced transitions from oscillatory to oxidized steady states. This type of transition was already shown in Figures 3A and 4A, chart b at the flow rate of 1.38×10^{-3} s^{-1}. Under high flow rate conditions, the state diagram shows transitions from oscillatory to reduced steady states, then transitions from reduced steady states to oxidized steady states with increasing the light intensity. Numerical calculations under different solute compositions exhibited different state diagrams (not shown); no transitions from oscillatory to reduced steady states were exhibited under the highly oxidative solute composition (condition a in Table 1), and no transitions from oscillatory to oxidized steady states were exhibited under the highly reductive solute composition (condition e in Table 1).

VI. Discussion

In terms of the experimental measurement, the optical absorption due to $Ru(bpy)_3^{3+}$ can directly be converted to the concentration. The redox potentials, on the other hand, may follow other reactions than the redox reactions of the catalyst, for instance, radical reactions in the mixtures. In terms of the simulation, the present model exhibits a realistic range of the concentrations of the catalyst, while the Nernst equation, i.e., $f(Z) = (RT/F)\ln(Z/(C_0 - Z))$, only gives relative changes (not absolute values) in the redox potentials. Thus using the optical absorbance, i.e., concentration of $Ru(bpy)_3^{3+}$, is preferable to compare the experimental results with the simulated results quantitatively.

The measurement of the optical absorbance in the present study showed that not all amount of the catalyst was oxidized at the plateau in the oscillations (Figure 2A, chart a) under the highly oxidative solute composition. In contrast, the simulated results exhibited complete oxidation of the catalyst at the plateau under the above condition. Other discrepancies in the amplitudes and waveforms of oscillations are also seen between experimental and simulated results under different solute compositions. In the simulation, the maximum concentration of the oxidized catalyst can be kept small if the rate constant in step O3b is set to a small value, or step O3b is changed to be reversible. However, in case of $Ru(bpy)_3^{2+}$ and ferroin catalysts with low redox potentials, i.e., $Ru(bpy)_3^{2+}/Ru(bpy)_3^{3+}$ (1.26 V) and $Fe(phen)_3^{2+}/Fe(phen)_3^{3+}$ (1.14 V), the reaction between the reduced form of catalysts and $BrO_2^\bullet$ (step O3b) has been reported to be irreversible.[24,32,40,41] In addition, the value (8×10^6 M^{-2} s^{-1}) of rate constant in step O3b adopted in the present simulation is nearly the same as that (4×10^6 M^{-2} s^{-1}) experimentally obtained in another study of $Ru(bpy)_3^{2+}$/BrMA/BrO_3^-/H_2SO_4 system.[24] To examine the role of step O3b on

TABLE 4: Values of Parameters Used in the Numerical Calculations

rate constants:	ref.
$k_{O1} = 2\,H^2$ ($M^{-1}\,s^{-1}$)	36
$k_{O2} = 3 \times 10^6\,H$ ($M^{-1}\,s^{-1}$)	36
$k_{O3a} = 42\,H$ ($M^{-1}\,s^{-1}$)	36
$k_{O-3a} = 4.2 \times 10^7$ ($M^{-1}\,s^{-1}$)	36
$k_{O3b} = 8 \times 10^6\,H$ ($M^{-1}\,s^{-1}$)	24, 36
$k_{O4} = 3 \times 10^3$ ($M^{-1}\,s^{-1}$)	36
$k_{O6} = 2 \times 10^{-3}$ (s^{-1})	29
$k_{-L0}/k_{L1} = 0.0223$ (M^2)	29, 39
$k_{L2'}/k_{L1} = 5.54$ (M^{-1})	29, 39

adjustable parameters: assigned arbitrarily in this work

run	k_{O5} (s^{-1})	h
a	0.023	0.68
b	0.1	0.67
c	0.18	0.57
d	1.05	0.516
e	1.1	0.504

initial conditions and constant concentrations

$X_0 = 0$ (M)	$V_{in} = 0$ (M)
$Y_0 = 1 \times 10^{-6}$ (M)	$Y_{in} = 0.05$ (mM)
$Z_0 = 0$ (M)	$C_0 = 0.1$ (mM)
$W_0 = 0$ (M)	$H = 0.6$ (M)
$V_0 = 0$ (M)	

the system behavior, we carried out numerical calculations with several sets of the rate constants k_{O3b} and different values of the adjustable parameters k_{O5} and h. However, the calculations did not reproduce results better than those already shown in the previous section.

The production of BrMA is represented by step O6 in which BrMA is generated via bromination of MA by intermediate species HOBr[20,37]

$$\mathrm{MA} + \mathrm{HOBr} \rightarrow \mathrm{BrMA} + \mathrm{H_2O} \qquad \text{(A12)}$$

where the number of the reaction step corresponds to that in the literature.[37] For the bromination of MA, another reaction may also occur[20,37]

$$\mathrm{MA} + \mathrm{Br_2} \rightarrow \mathrm{BrMA} + \mathrm{Br^-} + \mathrm{H^+} \qquad \text{(A11)}$$

To reflect the above reactions in the Oregonator scheme with a small modification of the previous model,[29] we simplified the two bromination reactions as step O6. The stoichiometric factor g ($= 1 - V/B_0$) represents the depletion of MA,[42] and is also introduced from a request of conservation of organic species; it guarantees the experimental constraint on [BrMA] ([BrMA] $< [CH_2(COOH)_2]_0$). It is noted that the production of Br^- in step A11 is included in step O5 in the present model.

The quasi-steady-state approximation for P in step O6 has been assumed as follows; The production rates for P, i.e., $r_{O1} + 2r_{O2} + r_{O4}$, in the present model are of the order of 10^{-6}∼10^{-5} M s^{-1} under the present oxidative and reductive solute conditions, respectively. On the other hand, the consumption rates for P in step O6 can be estimated to be of the order of 10^{-6}∼10^{-5} M s^{-1} under the oxidative and reductive solute conditions, respectively, by employing the above reactions A11 and A12 with the reported rate constants:[37] $k_{A11} = 40$ M $s^{-1}$and $k_{A12} = 8.2$ M s^{-1}. In this estimation, the concentrations of the intermediate species [HOBr] and [Br_2] are assumed to be of the order of 10^{-5}∼10^{-6} M that are nearly the same as the values of X, Y, and W in the present model. In this way, if we admit this steady-state approximation for P, the rate for step O6 can be replaced by the sum of the rates for steps O1, O2, and O4 as listed in Table 2; the production rate for V is multiplied by g ($= 1 - V/B_0$) as compared with that in the previous model.[29] It is noted that this factor substantially improves quantitative agreement with experimental constraint on the conservation of the organic species, however, it does not qualitatively affect the results obtained in the previous model.[29,43]

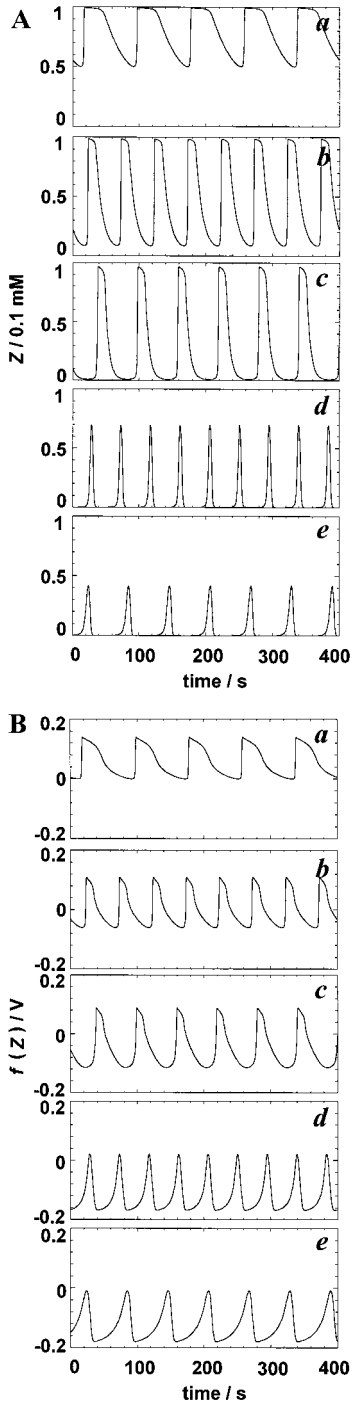

Figure 4. Simulated results of oscillatory behavior in $Z = [Ru(bpy)_3^{3+}]$ (A), and in the function of $f(Z) = (RT/F)\ln(Z/(C_0\text{-}Z))$ (B) under dark conditions. Charts a, b, c, d, and e correspond to the same alphabetical charts in Figure 2. Solute concentrations and the value of the flow rate used in each simulation were the same as those used in each experiment. The values of the other parameters are listed in Table 4. R (8.31 J K^{-1} mol^{-1}) is the gas constant, F (96 500 C mol^{-1}) is the Faraday constant, T (298 K) is the absolute temperature, and C_0 (0.1 mM) is the total concentration of the catalyst.

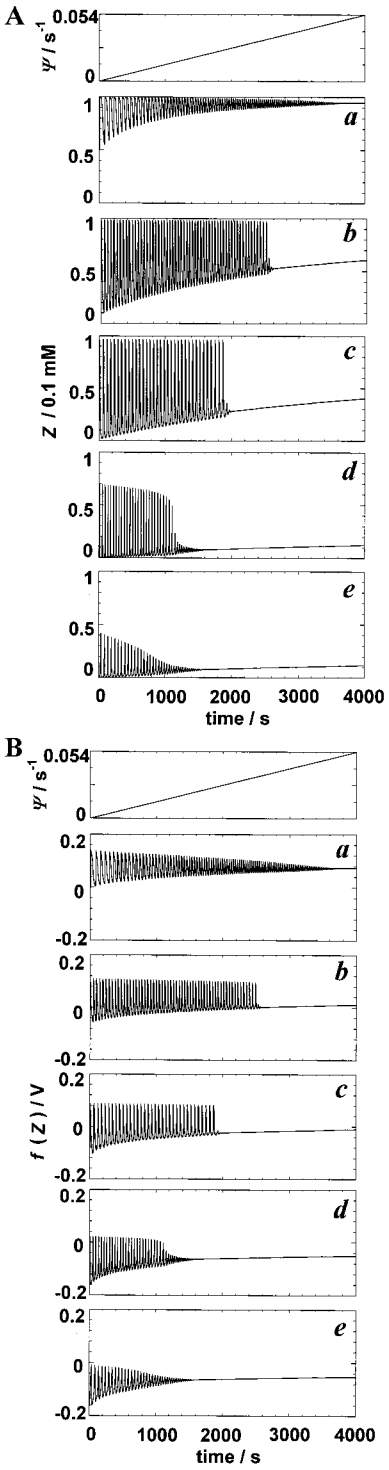

Figure 5. Simulated results of transitions from oscillatory to steady-state behavior in $Z = [Ru(bpy)_3^{3+}]$ (A), and in the function of $f(Z) = (RT/F)\ln(Z/(C_0-Z))$ (B) under laser irradiation. The intensity of light was changed linearly as shown in the top chart in this figure. Charts a, b, c, d, and e correspond to the same alphabetical charts in Figure 3. Simulated conditions were the same as those listed in the caption of Figure 4 except for the light irradiation.

The improvement of step L0 is based on photochemistry;[38] the concentration of the ground state of the catalyst should be taken into account in the production rate of the excited state of the catalyst under light irradiation. This improvement guarantees that no light is absorbed after the catalyst is oxidized completely even if the light intensity is increased further. As a result of the two modifications together with the modification of step O3,

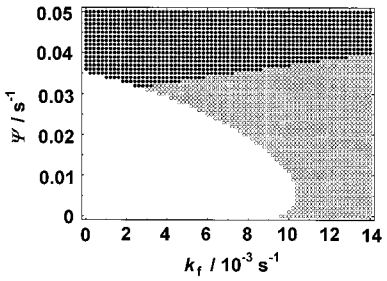

Figure 6. State diagram obtained by numerical integration of the present model under a condition of run b listed in Tables 1 and 4. Control parameters were the light intensity (Ψ) and the flow rate (k_f) in the model. White region, open circles (○), and closed circles (●) indicate oscillations, reduced steady states, and oxidized steady states, respectively. The reduced and oxidized steady states were defined as $Z \geq C_0/2$ and $Z < C_0/2$, respectively.

the photochemical terms $p_1(V, Z)$ and $p_2(V, Z)$ have been improved to reflect the realistic constraint on the concentrations compared with those in our previous model.[29]

The present model can indicate whether photoinduced steady states are oxidized or reduced by considering the values of Z and C_0. The previous model can represent nearly the same phase diagram[29] as shown in Figure 6, however, cannot indicate the character of the steady states. Hanazaki et al. have reported an experimentally obtained state diagram spanned by light power and concentrations of BrO_3^- for the photosensitive BZ reaction,[6] showing that the photoinduced steady states were oxidized states under high concentrations of BrO_3^-, and were reduced states under low concentrations of BrO_3^-. The present model also exhibited transitions from oscillatory to oxidized steady state behavior under the highly oxidative solute composition (condition a in Table 1), and transitions from oscillatory to reduced steady state behavior under the highly reductive solute composition (condition e in Table 1).[44]

In the present conditions, we observed neither irregular nor chaotic oscillations experimentally, and numerical calculations have never exhibited such oscillations either, even if the values of the flow rate have been changed. Separate calculations with different values of solute concentrations, flow rates, and the adjustable parameters (k_{O5} and h) have exhibited chaotic oscillations under light irradiation. However, the calculations have shown that photoinduced chaos can be generated under limited conditions in the present model as well as the previous model.[29] Kaminaga[45] and Mori et al.[9] have experimentally observed irregular oscillations in the $Ru(bpy)_3^{2+}$-catalyzed BZ reaction under light irradiation, however experiments in a longer time scale might be required to clarify the behavior as described in the literature.[9] Studies of chaos in the present model as well as in experiments are in progress in our laboratory.

VII. Conclusions and Remarks

Several types of oscillations, photoinduced transitions, and steady states were experimentally exhibited in different oxidative or reductive solute mixtures of the $Ru(bpy)_3^{2+}$-catalyzed BZ reaction. Some of the characteristic features of the behavior were oscillations with a plateau in an oxidized state under a highly oxidative solute composition, photoinduced abrupt and smooth transitions from oscillatory to steady states, and photoinduced oxidized and reduced steady states. The experimental behavior can be reproduced quantitatively by an Oregonator-class model of the BZ reaction improved to represent realistic range of concentrations of both the catalyst and bromomalonic acid. The

photochemical terms in the present model have also been improved to reflect the experimental constraint on the concentrations.

Numerical studies of the present model indicate that photoinduced chaos in this system may be exhibited under very limited experimental conditions. The photoinduction, i.e., transitions from steady state to oscillatory behavior, has been shown to lead to the chaos according to the calculations. At present, we assume that an appropriate ratio of $[BrO_3^-]$/[MA] that is neither highly oxidative nor reductive may give rise to photoinduced chaos in experiments. Modification of the condition d in Table 1 in the present study, where several oscillations with small amplitudes appeared just before the transition from oscillatory to steady-state behavior, may be one of the candidates for the generation of the chaos.

Recent studies have shown new stages in the mechanism of the photosensitive BZ reaction. Vanag et al. reported that dibromomalonic acid ($CBr_2(COOH)_2$) also reacts with $*Ru(bpy)_3^{2+}$ and produces Br^-.[46] On the other hand, the photoinduction may occur via other reactions than the direct reaction between BrO_3^- and $*Ru(bpy)_3^{2+}$.[47] These studies prove that there is more to learn about photochemical cycles in the photosensitive BZ reaction.

Finally, we refer to an application of such a modeling study of nonlinear chemical reaction systems. Complex chemical reactions can be found, for instance, in the area of environmental or atmospheric systems,[48] and the modeling and analytical methods of nonlinear chemical dynamics have been applied to the systems.[49,50] Recent studies have found chaos in the concentrations of chemical species such as H, HO_x, O_x, CO, and NO_x in a model of photochemistry in the mesosphere,[49] or in the troposphere.[50] Modeling and analytical studies of small systems such as the BZ reaction can be very useful for understanding dynamic behavior in more complex and larger systems appearing in the field of such as environmental science.

Acknowledgment. We thank Dr. Noriaki Okazaki for his advise for the experimental setup.

References and Notes

(1) Belousov, B. P. In *Oscillations and Traveling Waves in Chemical Systems*; Field, R. J., Burger, M., Eds.; John Wiley and Sons: New York, 1985; pp 605−613.

(2) Zaikin, A. N.; Zhabotinsky, A. M. *Nature* **1970**, *225*, 535−537.

(3) Demas, J. N.; Diemente, D. *J. Chem. Edu.* **1973**, *50*, 357−356.

(4) Srivastava, P. K.; Mori, Y.; Hanazaki, I. *Chem. Phys. Lett.* **1992**, *190*, 279−284.

(5) Jinguji, M.; Ishihara, M.; Nakazawa, T. *J. Phys. Chem.* **1992**, *96*, 4279−4281.

(6) Hanazaki, I.; Mori, Y.; Sekiguchi, T.; Rábai, G. *Physica D* **1995**, *84*, 228−237.

(7) Reddy, M. K. R.; Szlávik, Z.; Ungvarai-Nagy, Zs.; Müller, S. C. *J. Phys. Chem.* **1995**, *99*, 15 081−15 085.

(8) Kádár, S.; Amemiya, T.; Showalter, K. *J. Phys. Chem.* **1997**, *101*, 8200−8206.

(9) Mori, Y.; Nakamichi, Y.; Sekiguchi, T.; Okazaki, N.; Matsumura, T.; Hanazaki, I. *Chem. Phys. Lett.* **1993**, *211*, 421−424.

(10) Sørensen, P. G.; Lorenzen, T.; Hynne, F. *J. Phys. Chem.* **1996**, *100*, 19 192−19 196.

(11) Agladze, K.; Obata, S.; Yoshikawa, K. *Physica D* **1995**, *84*, 238−245.

(12) Matsumura-Inoue, T.; Nakamura, T.; Mori, Y.; Hanazaki, I. *Chem. Lett.* **1999**, 1237−1238.

(13) Treindl, L.; Knudsen, D.; Nakamura, T.; Matsumura-Inoue, T.; Jørgensen, K. B.; Ruoff, P. *J. Phys. Chem. A* **2000**, *104*, 10 783−10 788.

(14) Kaminaga, A.; Mori, Y.; Hanazaki, I. *Chem. Phys. Lett.* **1997**, *279*, 339−343.

(15) Matsumura-Inoue, T.; Nakamichi, Y.; Yamaguchi, T. *ACH−Models Chem.* **1998**, *135*, 305−313.

(16) Yamaguchi, T.; Shimamoto, Y.; Amemiya, T.; Yoshimoto, M.; Ohmori, T.; Nakaiwa, M.; Akiya, T.; Sato, M.; Matsumura-Inoue, T. *Chem. Phys. Lett.* **1996**, *259*, 219−224.

(17) Sekiguchi, T.; Mori, Y.; Okazaki, N.; Hanazaki, I. *Chem. Phys. Lett.* **1994**, *219*, 81−85.

(18) Kaminaga, A.; Hanazaki, I. *Chem. Phys. Lett.* **1997**, *278*, 16−20.

(19) Kaminaga, A.; Hanazaki, I. *J. Phys. Chem. A* **1998**, *102*, 3307−3314.

(20) Field, R. J.; Körös, E.; Noyes, R. M. *J. Am. Chem. Soc.* **1972**, *94*, 8649−8664.

(21) Györgyi, L.; Turányi, T.; Field, R. J. *J. Phys. Chem.* **1990**, *94*, 7162−7170.

(22) Försterling, H.-D.; Murányi, S.; Noszticzius, Z. *J. Phys. Chem.* **1990**, *94*, 2915−2921.

(23) Field, R. J.; Noyes, R. M. *J. Chem. Phys.* **1974**, *60*, 1877−1884.

(24) Gao, Y.; Försterling, H.-D. *J. Phys. Chem.* **1995**, *99*, 8638−8644.

(25) Zeyer, K.-P.; Schneider, F. W. *J. Phys. Chem. A* **1998**, *102*, 9702−9709.

(26) Solli, G. M.; Ruoff, P. *J. Chem. Phys.* **1995**, *103*, 1440−1447.

(27) Amemiya, T.; Ohmori, T.; Nakaiwa, M.; Yamaguchi, T. *J. Phys. Chem. A* **1998**, *102*, 4537−4542.

(28) Amemiya, T.; Ohmori, T.; Nakaiwa, M.; Yamamoto, T.; Yamaguchi, T. *J. Biol. Phys.* **1999**, *25*, 73−85.

(29) Amemiya, T.; Ohmori, T.; Yamaguchi, T. *J. Phys. Chem. A* **2000**, *104*, 336−344.

(30) Okazaki, N.; Mori, Y.; Hanazaki, I. *J. Phys. Chem.* **1996**, *100*, 14 941−14 948.

(31) Smoes, M.-L. *J. Chem. Phys.* **1979**, *71*, 4669−4679.

(32) Zhabotinsky, A. M.; Buchholtz, F.; Kiyatkin, A. B.; Epstein, I. R. *J. Phys. Chem.* **1993**, *97*, 7578−7584.

(33) Yoshida, R.; Tanaka, M.; Onodera, S.; Yamaguchi, T.; Kokufuta, E. *J. Phys. Chem. A* **2000**, *104*, 7549−7555.

(34) Showalter, K.; Noyes, R. M.; Bar-Eli, K. *J. Chem. Phys.* **1978**, *69*, 2514−2524.

(35) Tyson, J. J. *J. Phys. Chem.* **1982**, *86*, 3006−3012.

(36) Field, R. J.; Försterling, H.-D. *J. Phys. Chem.* **1986**, *90*, 5400−5407.

(37) Györgyi, L.; Field, R. J. *J. Phys. Chem.* **1991**, *95*, 6594−6602.

(38) Hanazaki, I. *J. Phys. Chem.* **1992**, *96*, 5652−5657.

(39) The value of k_{-L0}/k_{L1} was 0.0329 in the previous paper,[29] however, was set to 0.0223 in the present paper. We recalculated the value of k_{-L0}/k_{L1} by using the concentration (0.25 M) of H_2SO_4 employed to determine the value of $k_{-L0}/(k_{L1}[H^+])$ in the literature.[8] The previous value of 0.0329 was obtained by using the concentration (0.37 M) of H_2SO_4 employed for the oscillatory experiments in the literature.[8] This change in the value of k_{-L0}/k_{L1} has been found to affect little the whole contents of the previous paper;[29] shifting the values of the light flux (Φ) has generated behavior virtually the same as that reported previously. The value of $k_{L2'}/k_{L1}$ was also found to be changed from 5.54 to 3.74 when we recalculated it in the same way. However, we still set it to 5.54 in the present paper because the original value (2.05) of $k_{L2}[H^+]'^2/(k_{L1}[H^+])$, where $[H^+]' = 0.37$ M and $[H^+] = 0.25$ M, was an adjustable parameter,[8] and both the values (5.54 and 3.74) have been found to generate practically the same behavior reported in the literature.[8] Note that the rate constant $k_{L2'}$ in this paper is the same as k_{L2} in the previous paper, because step L2′ has been assumed to be rate determining in step L2 in the previous paper.[29]

(40) Rovinsky, A. B.; Zhabotinsky, A. M. *J. Phys. Chem.* **1984**, *88*, 6081−6084.

(41) Kuhnert, L.; Krug, H.-J. *J. Phys. Chem.* **1987**, *91*, 730−733.

(42) Calculations by using the present model have shown that the concentration of MA is maximally depleted to 75% of the initial concentration under the oxidative solute condition. On the other hand, the depletion of the inorganic species, i.e., BrO_3^-, is very small; it is maximally 3% of the initial concentration under the reductive condition. Thus, the concentration of BrO_3^- can be assumed to be constant in the model.

(43) Without the factor $1-V/B_0$, the values of V have been found to exceed B_0 under a condition of low flow rates with light irradiation. For instance, they exceed the inflow concentration (7.5 mM) of malonic acid (MA) under a condition listed in the captions of Figures 3 and 4 in our previous paper,[29] at a flow rate of 1×10^{-4} s^{-1}. Except for this behavior, the both models can give qualitatively the same results with small tuning of the values of the adjustable parameters.

(44) To simulate the state diagram spanned by light power and $[BrO_3^-]$ reported by Hanazaki et al.,[6] we have to determine the values of adjustable parameters k_{O5} and h depending on $[BrO_3^-]$ by separate experiments. We did not carry out such experiments, however, tried to simulate the state diagram with constant values of k_{O5} and h independent of $[BrO_3^-]$, and obtained qualitatively similar shape of the diagram reported by Hanazaki et al.[6]

(45) Kaminaga, A. Ph.D. Thesis, Graduate University for Advanced Studies, 1997.

(46) Vanag, V. K.; Zhabotinsky, A. M.; Epstein, I. R. *J. Phys. Chem. A*

2000, *104*, 8207−8215.
(47) Matsumura-I., T., Private communication.
(48) *Atmospheric Chemistry: Measurements, Mechanisms and Models, Faraday Discuss.* **1995**, *100*.
(49) Johnson, B. R.; Scott, S. K.; Tinsley, M. R. *J. Chem. Soc., Faraday Trans.* **1998**, *94*, 2709−2715.
(50) Field, R. J.; Hess, P. G.; Kalachev, L. V.; Madronich, S. *J. Geophys. Res.* **2001**, *106D*, 7553−7565.